

I. TITLE

The signature of topology in polar and chiral non-magnetic crystal classes

II. AUTHOR LIST

Giancarlo Soavi^{1,2,*} and Jan Wilhelm^{3,4,†}

III. AFFILIATIONS

¹Institute of Solid State Physics, Friedrich Schiller University Jena, Helmholtzweg 5, 07743 Jena, Germany

²Abbe Center of Photonics, Friedrich Schiller University Jena, Albert-Einstein-Straße 6, 07745 Jena, Germany

³Institute of Theoretical Physics, University of Regensburg, 93053 Regensburg, Germany

⁴Regensburg Center for Ultrafast Nanoscopy (RUN), University of Regensburg, 93053 Regensburg, Germany

* giancarlo.soavi@uni-jena.de † jan.wilhelm@physik.uni-regensburg.de

IV. ABSTRACT

Topology is fundamental to condensed matter physics, underlying phenomena such as the quantum Hall effect in its various forms, protected surface states and spin-valley locking. Central to this is the Berry curvature, a measure of the geometric properties of Bloch wavefunctions in crystals. Despite its established connections to space inversion and time-reversal symmetries, a comprehensive framework linking the Berry curvature to other crystal symmetries is still missing. Here, we present a theoretical model for the Jacobian matrix of the Berry curvature in the proximity of optical resonances for all non-magnetic crystal classes. The Jacobian matrix of the Berry curvature is readily derived from the second-order nonlinear optical susceptibilities of the time-invariant point groups. We show that the diagonal elements of the Jacobian matrix, which define the divergence of the Berry curvature, are non-zero only for the chiral crystal classes, pointing towards a topological origin of circular dichroism. In polar crystals, we uniquely find a non-zero curl of the Berry curvature, suggesting a topological origin of spontaneous polarization *via* the Maxwell-Berry equations. Our findings thus open new perspectives for the topological interpretation of textbook phenomena at the heart of condensed matter physics.

V. MAIN TEXT

In modern condensed matter physics, several phenomena, such as the quantum Hall effect in its various forms [1, 2], spontaneous polarization and ferroelectricity, the manifestation of Weyl and Dirac fermions, are interpreted on the basis of topological quantities [3]. Among those, the Berry curvature $\mathbf{\Omega}(\mathbf{k})$ plays a crucial role. The Berry curvature can be readily linked to the space inversion, time reversal and energy-spin properties of crystals *via* simple and effective rules. For instance, crystals where space inversion symmetry (SIS) is preserved must obey $E_{\uparrow}(+\mathbf{k}) = E_{\uparrow}(-\mathbf{k})$ and $\mathbf{\Omega}(\mathbf{k}) = \mathbf{\Omega}(-\mathbf{k})$. Similarly, when time-reversal symmetry (TRS) is preserved one obtains $E_{\uparrow}(+\mathbf{k}) = E_{\downarrow}(-\mathbf{k})$ and $\mathbf{\Omega}(\mathbf{k}) = -\mathbf{\Omega}(-\mathbf{k})$ [3, 4]. With these expressions, it is already possible to qualitatively explain a large number of fascinating phenomena, such as spin-valley locking in transition metal dichalcogenides (TMDs) and its consequences for transport [5] and nonlinear optical measurements [6], or even non-trivial spin textures at the surfaces of topological materials [7].

In a broader perspective, and given the relevance of topology for solid-state physics, one might expect the existence of a direct relation between any type of symmetry dictated by crystal classes (*e.g.*, mirror, rotation, improper rotation *etc.*) and the Berry curvature, as for SIS and TRS. However, such relation is surprisingly still missing. In this work, we fill this conceptual gap by providing rules for the Jacobian matrix of the Berry curvature $\mathbf{G} = \nabla_{\mathbf{k}}^T \boldsymbol{\Omega}(\mathbf{k})$ derived from the second order nonlinear susceptibility of the non-magnetic crystal classes. From this, we extract the divergence ($\nabla \cdot$) and curl ($\nabla \times$) of the Berry curvature for all the possible time-invariant point groups and we discuss their physical relevance for the chiral (C_n and D_n) and polar (C_n and C_{nv}) crystals. We find that only in the chiral point groups (with the only exception of the T and O groups), all elements of $\nabla_{\mathbf{k}} \cdot \boldsymbol{\Omega}$ are non-zero, and we interpret this as the topological origin of circular dichroism. We confirm our rules for the chiral crystal trigonal Tellurium (t-Te) using $\boldsymbol{\Omega}(\mathbf{k})$ computed from density functional theory (DFT) [8, 9]. Moreover, we find that $\nabla_{\mathbf{k}} \times \boldsymbol{\Omega} \neq 0$ only in the polar crystal classes, and that a non-zero $(\nabla_{\mathbf{k}} \times \boldsymbol{\Omega})_{\alpha}$ along $\alpha = x, y, z$ is equivalent to the presence of a polar axis in the crystal along the α direction. We interpret this on the basis of the recently published Maxwell-Berry equations [10], indicating that the existence of the spontaneous polarization in polar crystals directly implies a rotation of the Berry curvature around the axis of the frequency-dispersive artificial electric field (AEF) [10, 11].

We envision that our results will provide a new platform to explore and understand the topological nature of symmetries in solid state physics.

Definitions and relation between the Berry curvature and non-magnetic crystal classes. The nonlinear optical (NLO) response of non-magnetic crystals is fully captured by their nonlinear tensors. In particular, for second harmonic generation (SHG) the $\chi^{(2)}$ tensor connects the nonlinear polarization response $\mathbf{P}^{(2)}(2\omega)$ of a material to the driving monochromatic electric field $\mathbf{E}(\omega)$,

$$P_{\gamma}^{(2)}(2\omega) = \sum_{\alpha\beta} \chi_{\gamma\beta\alpha}^{(2)} E_{\beta}(\omega) E_{\alpha}(\omega), \quad (1)$$

where $\alpha, \beta, \gamma \in \{x, y, z\}$ are Cartesian coordinates. The symmetry properties of the $\chi^{(2)}$ tensor are intrinsically linked to the symmetry of the crystal lattice where the nonlinear optical processes occur: due to symmetry, many of the 27 tensor elements $\chi_{\gamma\beta\alpha}^{(2)}$ are either

zero or non-independent [12]. The Neumann's principle suggests that the structure of such tensors directly links to the symmetry of a material in its ground state [13]. Our model starts from here: we first find a relation between the Berry curvature and the elements of a generic $\chi^{(2)}$ tensor. In a 3D crystal and for a n band at the crystal momentum \mathbf{k} in the Brillouin zone (BZ), there are only three independent elements of the Berry curvature, defined as [14]:

$$\mathbf{\Omega}_n(\mathbf{k}) = \begin{pmatrix} \Omega_n^x \\ \Omega_n^y \\ \Omega_n^z \end{pmatrix} = \begin{pmatrix} \Omega_n^{yz}(\mathbf{k}) \\ \Omega_n^{zx}(\mathbf{k}) \\ \Omega_n^{xy}(\mathbf{k}) \end{pmatrix} = \nabla_{\mathbf{k}} \times \mathbf{d}_{nn}(\mathbf{k}), \quad (2)$$

where $\mathbf{d}_{nn}(\mathbf{k}) = i\langle u_{n\mathbf{k}} | \nabla_{\mathbf{k}} | u_{n\mathbf{k}} \rangle$ is the Berry connection and $u_{n\mathbf{k}}$ is the lattice-periodic part of a Bloch function [15]. From Eq. (2), we can define the Jacobian matrix $\mathbf{G} = \nabla_{\mathbf{k}}^T \mathbf{\Omega}(\mathbf{k})$, divergence $\nabla_{\mathbf{k}} \cdot \mathbf{\Omega}$, and the curl $\nabla_{\mathbf{k}} \times \mathbf{\Omega}$ of the Berry curvature. Next, we recall the analytical expression of the $\chi^{(2)}$ tensor derived from microscopic nonlinear current responses [6, 16, 17]. This leads to an analytical expression for a generic element $\chi_{\gamma\beta\alpha}^{(2)}$ in the case of resonant SHG between a valence (v) and a conduction (c) band [18]:

$$\chi_{\gamma\beta\alpha}^{(2)} = C \int_{\text{BZ}} d\mathbf{k} \delta(\varepsilon_{cv} - 2\omega) d_{vc}^\gamma \left[\frac{\partial d_{cv}^\alpha}{\partial k_\beta} + i d_{cv}^\alpha (d_{cc}^\beta - d_{vv}^\beta) \right] \quad (3)$$

where C is a real-valued prefactor [16, 17] and ε_{cv} is the energy gap between valence and conduction band. Here, we have suppressed the dependency of ε_{cv} and d_{nm}^α on \mathbf{k} . To arrive at Eq. (3), we have considered resonant excitation ($\varepsilon_{cv} \approx 2\omega$) between a local maximum of the valence band and a local minimum of the conduction band ($\partial\varepsilon_{cv}/\partial k_\beta = 0$). Next, we observe from Eq. (3) (see online methods for a step-by-step derivation):

$$\text{Im} \left[\chi_{\alpha\beta\gamma}^{(2)} - \chi_{\gamma\beta\alpha}^{(2)} \right] = C \int_{\text{BZ}} d\mathbf{k} \delta(\varepsilon_{cv} - 2\omega) \frac{\partial}{\partial k_\beta} \text{Im} \left[d_{vc}^\alpha d_{cv}^\gamma \right]. \quad (4)$$

For a two-band model with a single valence band v and a single conduction band c , the Berry curvature $\mathbf{\Omega}(\mathbf{k})$ can be written as [19]:

$$\Omega^{\alpha\beta}(\mathbf{k}) = 2 \text{Im} [d_{vc}^\alpha(\mathbf{k}) d_{cv}^\beta(\mathbf{k})], \quad (5)$$

and thus Eq. (4) can be re-written as

$$\text{Im} \left[\chi_{\alpha\beta\gamma}^{(2)} - \chi_{\gamma\beta\alpha}^{(2)} \right] = \frac{C}{2} \int_{\text{BZ}} d\mathbf{k} \delta(\varepsilon_{cv} - 2\omega) \frac{\partial \Omega^{\alpha\gamma}}{\partial k_\beta}. \quad (6)$$

Note that Eq. (6) has a zero-frequency analogue which involves the Berry curvature dipole [20]. If we consider resonant driving at N_{res} resonances in the BZ ($\varepsilon_{cv}(\mathbf{k}_{\text{res}}^{(i)}) \approx 2\omega$, $i = 1, \dots, N_{\text{res}}$), the δ -function simplifies the integral to a sum over resonances:

$$\text{Im} \left[\chi_{\alpha\beta\gamma}^{(2)} - \chi_{\gamma\beta\alpha}^{(2)} \right] = \frac{C}{2} \sum_{i=1}^{N_{\text{res}}} \frac{\partial \Omega^{\alpha\gamma}}{\partial k_\beta} \Big|_{\mathbf{k}_{\text{res}}^{(i)}}. \quad (7)$$

For resonant driving at the Γ -point ($\mathbf{k}_{\text{res}}^{(1)} = 0$), there is only one single resonance ($N_{\text{res}} = 1$). Furthermore, since we only consider non-magnetic crystal classes where TRS is preserved, any resonance at $+\mathbf{k} \neq 0$ must have a counter-part at $-\mathbf{k}$ given the relation $E_\uparrow(+\mathbf{k}) = E_\downarrow(-\mathbf{k})$ and, thus, for $\mathbf{k} \neq 0$ we will have $N_{\text{res}} = 2$. We furthermore notice that $\Omega(\mathbf{k}) = -\Omega(-\mathbf{k})$ when TRS is preserved [3], which implies that $\partial \Omega^{\alpha\gamma} / \partial k_\beta$ is equal at opposite momenta $\pm \mathbf{k}$. Eq. (7) thus simplifies for $N_{\text{res}} \leq 2$,

$$\text{Im} \left[\chi_{\alpha\beta\gamma}^{(2)} - \chi_{\gamma\beta\alpha}^{(2)} \right] = \frac{CN_{\text{res}}}{2} \frac{\partial \Omega^{\alpha\gamma}}{\partial k_\beta} \Big|_{\text{res}}, \quad (8)$$

where $|_{\text{res}}$ indicates that the k_β -derivative needs to be taken at the corresponding optical resonance in the BZ. The derivation of Eq. (8) from Eq. (7) is obvious also from the fact that, when TRS is preserved, any $\chi_{\alpha\beta\gamma}^{(2)}$ element of the NLO susceptibility must be identical at energetically degenerate resonances with opposite momenta [6]. Since we are only considering resonant excitation, the elements of the $\chi^{(2)}$ tensor will be purely imaginary:

$$\chi_{\alpha\beta\gamma}^{(2)} - \chi_{\gamma\beta\alpha}^{(2)} = 2\tilde{C} \frac{\partial \Omega^{\alpha\gamma}}{\partial k_\beta} \Big|_{\text{res}}, \quad (9)$$

where $\tilde{C} = iCN_{\text{res}}/4$. We notice that Eq. (9) provides an elegant, simple and visual approach to calculate the Jacobian matrix of the Berry curvature at resonances in the BZ,

$\alpha \backslash \beta\gamma$	xx	yy	zz	yz, zy	xz, zx	xy, yx
x	$d_{11}^{(2)}$	$d_{12}^{(2)}$	$d_{13}^{(2)}$	$d_{14}^{(2)}$	$d_{15}^{(2)}$	$d_{16}^{(2)}$
y	$d_{21}^{(2)}$	$d_{22}^{(2)}$	$d_{23}^{(2)}$	$d_{24}^{(2)}$	$d_{25}^{(2)}$	$d_{26}^{(2)}$
z	$d_{31}^{(2)}$	$d_{32}^{(2)}$	$d_{33}^{(2)}$	$d_{34}^{(2)}$	$d_{35}^{(2)}$	$d_{36}^{(2)}$

	∇_{k_x}	∇_{k_y}	∇_{k_z}
Ω_v^x	$\frac{\partial \Omega_v^x}{\partial k_x} = \frac{d_{25}^{(2)} - d_{36}^{(2)}}{\tilde{c}}$	$\frac{\partial \Omega_v^x}{\partial k_y} = \frac{d_{24}^{(2)} - d_{32}^{(2)}}{\tilde{c}}$	$\frac{\partial \Omega_v^x}{\partial k_z} = \frac{d_{23}^{(2)} - d_{34}^{(2)}}{\tilde{c}}$
Ω_v^y	$\frac{\partial \Omega_v^y}{\partial k_x} = \frac{d_{31}^{(2)} - d_{15}^{(2)}}{\tilde{c}}$	$\frac{\partial \Omega_v^y}{\partial k_y} = \frac{d_{36}^{(2)} - d_{14}^{(2)}}{\tilde{c}}$	$\frac{\partial \Omega_v^y}{\partial k_z} = \frac{d_{35}^{(2)} - d_{13}^{(2)}}{\tilde{c}}$
Ω_v^z	$\frac{\partial \Omega_v^z}{\partial k_x} = \frac{d_{16}^{(2)} - d_{21}^{(2)}}{\tilde{c}}$	$\frac{\partial \Omega_v^z}{\partial k_y} = \frac{d_{12}^{(2)} - d_{26}^{(2)}}{\tilde{c}}$	$\frac{\partial \Omega_v^z}{\partial k_z} = \frac{d_{14}^{(2)} - d_{25}^{(2)}}{\tilde{c}}$

FIG. 1. (Top) Generic nonlinear tensor $\chi^{(2)}$ for SHG in the contracted notation [12]. (Bottom) Relation between the elements of the NLO tensor and the derivatives of the Berry curvature along all \mathbf{k} directions at optical resonances based on Eq. (9)/(1).

$$\mathbf{G} = \nabla_{\mathbf{k}}^T \Omega(\mathbf{k}) = \begin{pmatrix} g_{xx} & g_{xy} & g_{xz} \\ g_{yx} & g_{yy} & g_{yz} \\ g_{zx} & g_{zy} & g_{zz} \end{pmatrix}, \quad g_{\alpha\beta} = \frac{\partial \Omega^\alpha}{\partial k_\beta}, \quad (10)$$

where we use a single spatial dimension α for the Berry curvature following Eq. (2). In Eq. (10) and subsequent equations, we omit $|_{\text{res}}$ at $\partial \Omega^\alpha / \partial k_\beta$ to ensure a more concise notation. Finally, we notice that our model considers only SHG, which allows us to freely exchange the two last indices, $\chi_{\alpha\beta\gamma}^{(2)} = \chi_{\alpha\gamma\beta}^{(2)}$, and thus to use the contracted notation for $d_{pq}^{(2)} = \frac{1}{2} \chi_{\alpha\beta\gamma}^{(2)}$ ($p = 1, 2, 3; q = 1, 2, \dots, 6$; Fig. 1).

The Jacobian matrix, divergence, and curl of the Berry curvature for the non-magnetic crystal classes. Based on eq. (9) and using the existing tables of $\mathbf{d}^{(2)}$ [12, Fig. 1.5.3], it is possible to immediately gain a general picture of the interplay between point group symmetries and Berry curvature. To do this, we write the rank 2 tensor \mathbf{G} for all the possible 32 non-magnetic (time-invariant) crystal classes.

For the crystal classes $D_{3h}, C_{3h}, T, T_d, O$ (5 groups) and for all the centro-symmetric crystal classes (11 groups), every element of \mathbf{G} is zero. In contrast, for the crystal class

C_1 , every element of \mathbf{G} is non-zero and independent. All the other 15 crystal classes can be grouped in four categories. For the crystal classes S_4 and D_{2d} there are only two independent elements of \mathbf{G} :

$$\mathbf{G}_{S_4} = \mathbf{G}_{D_{2d}} = \begin{pmatrix} g_{xx} & g_{xy} & 0 \\ g_{xy} & -g_{xx} & 0 \\ 0 & 0 & 0 \end{pmatrix} \quad (11)$$

with $g_{xy} = 0$ in the crystal class D_{2d} . For the C_n ($n \geq 2$, 4 groups) crystal classes we find:

$$\mathbf{G}_{C_{n,n \geq 2}} = \begin{pmatrix} g_{xx} & g_{xy} & g_{xz} \\ -g_{xy} & g_{yy} & 0 \\ g_{zx} & 0 & g_{zz} \end{pmatrix} \quad (12)$$

with the additional relations $g_{xx} = g_{yy} = -\frac{1}{2}g_{zz}$ and $g_{xz} = g_{zx} = 0$ for $n \geq 3$, and $g_{xy} = 0$ for $n = 2$. For the D_n (4 groups) crystal classes we find:

$$\mathbf{G}_{D_n} = \begin{pmatrix} g_{xx} & 0 & 0 \\ 0 & g_{yy} & 0 \\ 0 & 0 & g_{zz} \end{pmatrix} \quad (13)$$

with the additional relation $g_{xx} = g_{yy} = -\frac{1}{2}g_{zz}$ for $n \geq 3$. Finally, for the C_{nv} (5 groups, where we take $C_{1h} = C_{1v}$) crystal classes we find:

$$\mathbf{G}_{C_{nv}} = \begin{pmatrix} 0 & g_{xy} & 0 \\ g_{yx} & 0 & g_{yz} \\ 0 & g_{zy} & 0 \end{pmatrix} \quad (14)$$

with the additional relations $g_{xy} = -g_{yx}$ for $n \geq 3$, and $g_{yz} = g_{zy} = 0$ for $n \geq 2$.

From \mathbf{G} , we can compute the divergence and the curl of the Berry curvature; the divergence is the trace of \mathbf{G} ,

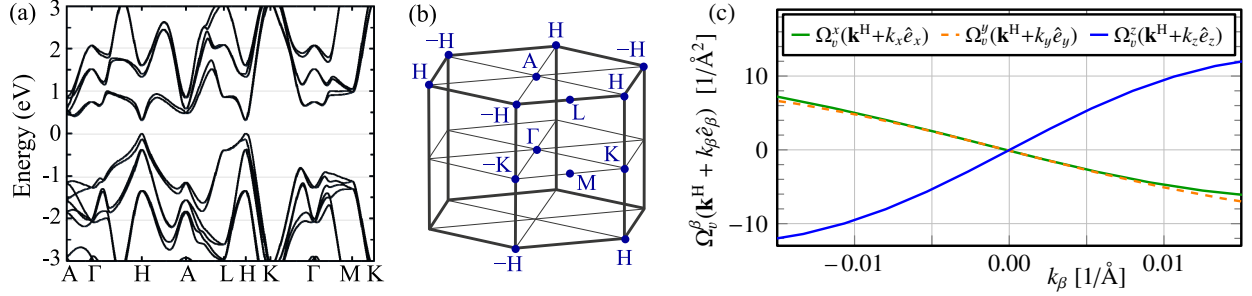


FIG. 2. (a) Band structure of t-Te calculated from DFT [8] and (b) Brillouin zone and high-symmetry points. (c) Berry curvature of the highest valence band close to the H-point in t-Te [9] along k_x, k_y, k_z ; \mathbf{k}^H denotes the crystal momentum of the H-point, \hat{e}_β is the unit vector along the coordinates $\beta \in \{x, y, z\}$. The derivatives of the Berry curvature at the H-point fulfill Eq. (20) within 3% accuracy.

$$\nabla_{\mathbf{k}} \cdot \boldsymbol{\Omega} = \sum_{\beta} g_{\beta\beta}, \quad (15)$$

where the three elements $g_{\beta\beta} = \partial\Omega^\beta/\partial k_\beta$ correspond to the case $\beta \neq \gamma \neq \alpha \neq \beta$ in Eq. (9). From the elements highlighted in orange in Fig. 1, it is trivial to validate $\nabla_{\mathbf{k}} \cdot \boldsymbol{\Omega} = 0$. Indeed, a non-zero divergence of the Berry curvature requires the presence of a Weyl point (band crossing) acting as a magnetic monopole [10] which is absent from our model. All other elements $d_{pq}^{(2)}$ highlighted in blue and green in Fig. 1 define the off-diagonal elements of \mathbf{G} , and thus the curl of the Berry curvature:

$$(\nabla_{\mathbf{k}} \times \boldsymbol{\Omega})_\alpha = \sum_{\alpha\beta} \epsilon_{\alpha\beta\gamma} \frac{\partial\Omega^\gamma}{\partial k_\beta} = \sum_{\alpha\beta} \epsilon_{\alpha\beta\gamma} g_{\gamma\beta} \quad (16)$$

where $\epsilon_{\alpha\beta\gamma}$ is the Levi-Civita tensor. As we discuss in the following, $\nabla_{\mathbf{k}} \times \boldsymbol{\Omega} \neq 0$ only in polar crystal classes. Furthermore, we can immediately highlight that for all the C_{nv} , C_{nh} and D_{nh} crystal classes, every element of $\nabla_{\mathbf{k}} \cdot \boldsymbol{\Omega}$ is zero. Namely, the presence of horizontal and/or vertical mirror symmetries imposes that each component Ω_v^β of the Berry curvature will have a valley in the k_β direction in correspondence of direct-gap resonant transitions, as observed, for instance, in TMDs at the $\pm K$ valleys [21].

Divergence of the Berry curvature in chiral crystal classes. The term chirality defines structures where improper rotations are not symmetry operations [22, 23]. Chirality plays a key role in science, with an impact that spans from chemistry, to solid state physics, optics and photonics [24–27]. A recent theoretical framework that combines chirality and topology *via* $\mathbf{\Omega}(\mathbf{k})$ has predicted the existence of Kramers-Weyl fermions [28], which were then experimentally measured in t-Te [29]. In addition, all the chiral D_n crystal classes should host non-trivial radial spin textures [30], as confirmed by theoretical studies on trigonal Selenium (Se) and Te [31]. Here, based on Eq. (11)-(14), we notice that all and only the chiral C_n and D_n crystal classes share a peculiarity in $\nabla_{\mathbf{k}} \cdot \mathbf{\Omega}$, namely:

$$g_{\beta\beta} = \frac{\partial\Omega^\beta}{\partial k_\beta} \neq 0 \quad \text{for the chiral point groups } C_n, D_n, \quad (17)$$

$$g_{zz} = \frac{\partial\Omega^z}{\partial k_z} = 0 \quad \text{for point groups } S_4, D_{2d}, \quad (18)$$

$$g_{\beta\beta} = \frac{\partial\Omega^\beta}{\partial k_\beta} = 0 \quad \text{for all other point groups.} \quad (19)$$

In Eq. (18), z denotes the axis of highest rotational symmetry in the crystal. Thus, it is obvious that all and only the chiral C_n and D_n crystal classes have $g_{zz} \neq 0$. Furthermore, C_n and D_n groups with rotational symmetry $n \geq 3$ (which form the chiral space groups of class II [22]) always have $g_{xx} = g_{yy} = -\frac{1}{2}g_{zz}$:

$$\frac{\partial\Omega^x}{\partial k_x} = \frac{\partial\Omega^y}{\partial k_y} = -\frac{1}{2} \frac{\partial\Omega^z}{\partial k_z} \neq 0 \quad (C_n, D_n, n \geq 3). \quad (20)$$

Before we continue, we note that in the T and O point groups, each element of $\nabla_{\mathbf{k}} \cdot \mathbf{\Omega}$ is zero, despite the absence of improper rotations. Interestingly, even though the T crystal class is chiral, all the possible class III space groups built with this structure are achiral (tables 2 and 3 in Ref. [22]). Instead, the O group is the only non-centrosymmetric crystal class without piezoelectricity and vanishing SHG in all directions [12, 22], and we are not aware of any study of the Berry curvature for crystals belonging to this point group.

We now test the validity of Eq. (20) by analyzing the Berry curvature of the chiral crystal t-Te [8, 9, 31]. The chirality of t-Te arises from the arrangement of the Te atoms, which form helical spirals along the crystal trigonal axis. The resulting crystal symmetry is D_3 . t-Te

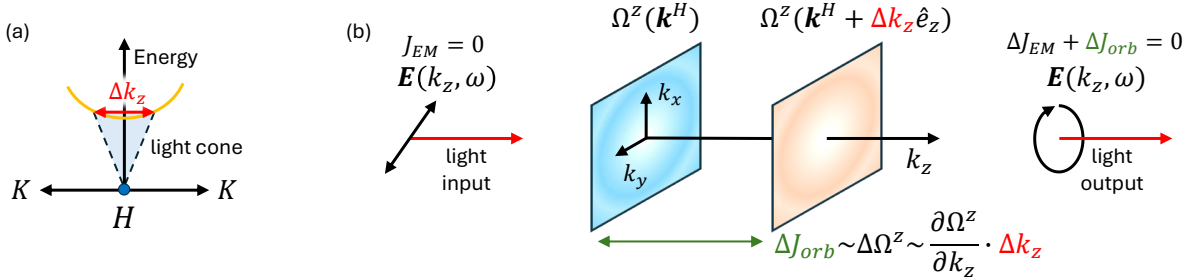


FIG. 3. Schematic of the topological origin of circular dichroism in C_n and D_n crystal classes. (a) Light cone giving rise to a momentum transfer Δk_z from the photon to the crystal. (b) The momentum of (resonant) photons along the k_z directions probes the non-zero derivative $\partial \Omega^z / \partial k_z$ of the Berry curvature, which then contributes to the conservation of the angular momentum *via* ΔJ_{orb} .

is a direct gap semiconductor with energy gap of ~ 0.3 eV calculated from DFT [8] close to the $\pm H$ point in the BZ (Fig. 2 a,b). Moreover, the valence band at $\pm H$ is non-degenerate, with opposite spins along the z direction in $\pm H$ [31], similar to the spin-valley locking of monolayer TMDs [21]. This is the ideal condition to test our model. Fig. 2 (c) shows the three components Ω_v^β of the Berry curvature at the $\pm H$ points of the BZ and along the three directions k_β , obtained for right-handed t-Te from Ref. [9]. From this, we have extracted the derivatives $\partial \Omega^\beta / \partial k_\beta|_{\pm H}$ and we found an agreement with Eq. (20) within 3% accuracy. In addition, we highlight that opposite enantiomers in chiral crystals will have opposite sign of $\chi_{xzy}^{(2)}$ [32], implying that also $\partial \Omega^z / \partial k_z$ will have opposite sign [33].

This observation reminds the change in sign of the Chern number in different enantiomers of the chiral semimetal PdGa [34], and the reversal of the polarity of the orbital angular momentum monopoles in chiral topological semimetals with opposite handedness [35]. Thus, this sign-flip of $\partial \Omega^z / \partial k_z$ could be the ultimate signature of handedness in topological chiral crystals [22].

Finally, we propose a physical interpretation of the results reported above. Summarizing Eq. (17)–(19) as

$$\frac{\partial \Omega^z}{\partial k_z} \begin{cases} \neq 0 & \text{for chiral point groups } C_n, D_n, \\ = 0 & \text{for chiral point groups } O, T, \\ = 0 & \text{for all other, non-chiral point groups,} \end{cases} \quad (21)$$

we have identified a unique fingerprint of all and only the C_n and D_n chiral point groups. We propose that this could be connected to the presence of circular dichroism, which is considered one of the best measures of chirality [22]. In particular, if we imagine an electromagnetic wave propagating in the z direction and with electric field oscillating in the x - y plane $\mathbf{E} = (E_x \hat{e}_x + E_y \hat{e}_y) e^{ik_z z}$, then we can state that only for the chiral C_n and D_n crystal classes the Ω^z component of the Berry curvature experienced by light will change (Fig. 3). The momentum Δk_z probed by light corresponds to the portion of the $\pm H$ resonance that falls within the light-cone (Fig. 3). This change in the Berry curvature can modify the selection rules for conservation of the angular momentum [36], and eventually leads to circular dichroism. Namely, the change in the angular momentum of the electromagnetic field ΔJ_{EM} caused by circular dichroism can be compensated by an orbital angular momentum ΔJ_{orb} proportional to $\Delta \Omega^z$ (Fig. 3) [37, 38].

Finally, it is interesting to notice that optical activity can occur also in the non-chiral point groups S_4 and D_{2d} , but not along the optic (z) axis [23]. Our model shows that in those point groups $g_{xx} = -g_{yy}$ and $g_{zz} = 0$ (Eq. 15), in agreement with the topological interpretation of circular dichroism discussed above.

Curl of the Berry curvature in polar crystal classes. A crystal class is defined as polar when it allows the existence of a permanent dipole moment and, thus, of an intrinsic spontaneous polarization [23]. There are 10 polar non-magnetic crystal classes, namely the C_n and C_{nv} point groups (where again we consider $C_{1h} = C_{1v}$). Ferroelectric crystals represent a subset of polar classes [13], where the spontaneous polarization can be switched with external electric fields. The modern theory of polarization [39] has demonstrated that this spontaneous electric dipole is closely related to the Berry phase of Bloch wavefunctions. Here, we extend and complement this topological interpretation of the spontaneous polarization by showing its connection to $\nabla_{\mathbf{k}} \times \boldsymbol{\Omega}$. We start from the observation (Eq. (11)-(14)):

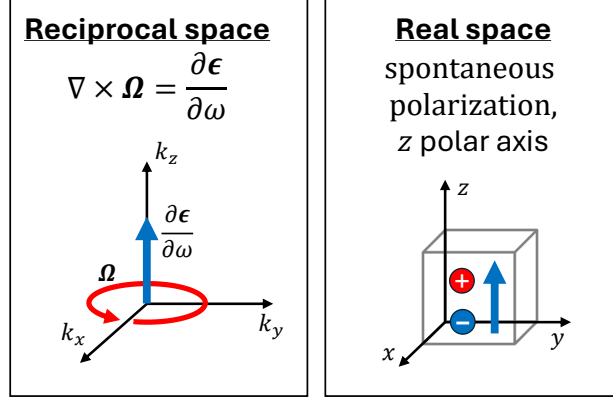


FIG. 4. Schematic of the topological origin of polarity in C_n and C_{nv} crystal classes. A polar axis, and thus a permanent spontaneous electric dipole, in the α direction in real space defines a rotation of Ω in a plane perpendicular to k_α in reciprocal space. This $\nabla_{\mathbf{k}} \times \Omega \neq 0$ originates from a frequency-dispersive artificial electric field in the k_α direction.

$$\nabla_{\mathbf{k}} \times \Omega \begin{cases} \neq 0 & \text{for all polar point groups } (C_n, C_{nv}), \\ = 0 & \text{for all other point groups.} \end{cases} \quad (22)$$

When we look closely at which elements of the vector $\mathbf{R} = \nabla_{\mathbf{k}} \times \Omega$ are non-zero in the different C_n and C_{nv} crystal classes, we find a one-to-one correspondence with the direction of the polar axis. Spontaneous polarization can only occur along a polar direction that has no symmetry-equivalent directions [23]. Based on the definition of the $\chi^{(2)}$ tensor and its symmetry axis from Ref. [12], the polar axis are $\alpha = x, y, z$ for C_1 , $\alpha = y$ for C_2 , $\alpha = x, z$ for C_{1v} , and $\alpha = z$ for all other polar point groups (see table 3.2.2.2 in Ref. [23]). Correspondingly, the vector $\mathbf{R} = \nabla_{\mathbf{k}} \times \Omega$ is non-zero in all directions for C_1 , while for the other polar point groups the non-zero elements are R_y for C_2 (Eq. (12)), R_x, R_z for C_{1v} (Eq. (14)), and R_z for all other polar crystal classes (Eq. (12) and (14)). Thus, for all C_n and C_{nv} crystal classes, a polar axis in the α direction in real space corresponds to a non-zero element R_α of $\nabla_{\mathbf{k}} \times \Omega$ in reciprocal space. Note that, for instance, a non-zero curl in the direction $R_z \neq 0$ implies a rotation of the Berry curvature in the k_x - k_y plane. The recently developed Maxwell-Berry equations [10] suggest that

$$\nabla_{\mathbf{k}} \times \Omega = \frac{\partial \epsilon}{\partial \omega} \quad (23)$$

where $\boldsymbol{\epsilon}$ is the electriclike Berry curvature [10] or artificial electric field (AEF) defined in Ref. [11]. Based on this, we can further infer that a spontaneous polarization in the α direction in real space produces a frequency-dispersive ϵ_α element of the AEF, which is then responsible of a rotation of the Berry curvature in a \mathbf{k} plane perpendicular to k_α (Fig. 4). Since $\nabla_{\mathbf{k}} \times \boldsymbol{\Omega}$ can now be measured with standard SHG experiments, our model provides a powerful approach to measure the AEF.

Conclusions. We have derived a general expression that relates the Berry curvature with the crystal symmetry for all non-magnetic point groups *via* the elements of the resonant second harmonic nonlinear susceptibility. From this, we extracted the derivative of the Berry curvature. We found that $\partial\Omega^\beta/\partial k_\beta \neq 0, \beta = x, y, z$ only for the C_n and D_n chiral crystal classes, while the presence of vertical and/or horizontal mirror symmetries implies that the Berry curvature has a valley at resonant k -points. Furthermore, we interpret the property $\partial\Omega^z/\partial k_z \neq 0$ of C_n and D_n chiral crystals as the one responsible of circular dichroism due to conservation of the angular momentum, and we propose that different enantiomers can be distinguished by a change in sign of $\partial\Omega^z/\partial k_z$. In addition, we found that $\nabla_{\mathbf{k}} \times \boldsymbol{\Omega} \neq 0$ only in the polar C_n and C_{nv} crystal classes, with non-zero elements R_α appearing only in presence of a spontaneous polarization along the α polar axis in real space. Thus, from the Maxwell-Berry equations [10], we propose that spontaneous polarization is also responsible of a non-zero ω derivative of the artificial electric field, which could be measured with standard SHG experiments. We envision that this work will contribute to the understanding of the interplay between symmetries and topology [40], and to the further development of topological nonlinear optics [17, 41, 42].

VI. ONLINE METHODS – ANALYTICAL CALCULATIONS

Definition of Berry curvature. For our analysis of the second-order non-linear optical susceptibility in terms of the Berry curvature, we introduce a single-electron Hamiltonian $h(\mathbf{k})$ with eigenstates $|n\mathbf{k}\rangle$ and eigenvalues $\epsilon_n(\mathbf{k})$,

$$h(\mathbf{k}) |n\mathbf{k}\rangle = \epsilon_n(\mathbf{k}) |n\mathbf{k}\rangle, \quad (24)$$

We also require dipole matrix elements

$$\mathbf{d}_{nn'}(\mathbf{k}) = i\langle n\mathbf{k} | \nabla_{\mathbf{k}} | n'\mathbf{k} \rangle. \quad (25)$$

We can project the dipole on an axis $\hat{\alpha}$,

$$d_{nn'}^{\alpha}(\mathbf{k}) = \mathbf{d}_{nn'}(\mathbf{k}) \cdot \hat{\alpha}. \quad (26)$$

The derivative of $d_{nn'}^{\alpha}(\mathbf{k})$ with respect to an axis $\hat{\beta}$ is:

$$\frac{\partial d_{nn'}^{\alpha}}{\partial k_{\beta}} = \hat{\beta} \cdot \nabla_{\mathbf{k}} d_{nn'}^{\alpha}(\mathbf{k}). \quad (27)$$

The BC $\Omega_{\alpha\beta}^n(\mathbf{k})$ of band n at \mathbf{k} for dimensions $\alpha, \beta \in \{x, y, z\}$ is defined as [3, Eq. (1.11)]

$$\Omega_n^{\alpha\beta}(\mathbf{k}) = \frac{\partial d_{nn}^{\beta}(\mathbf{k})}{\partial k_{\alpha}} - \frac{\partial d_{nn}^{\alpha}(\mathbf{k})}{\partial k_{\beta}}. \quad (28)$$

We conclude

$$\Omega_n^{\alpha\alpha}(\mathbf{k}) = 0 \quad \text{and} \quad \Omega_n^{\alpha\beta}(\mathbf{k}) = -\Omega_n^{\beta\alpha}(\mathbf{k}). \quad (29)$$

In a 3d crystal, there are thus only three independent elements of the Berry curvature, which are labelled as $\Omega_n^x, \Omega_n^y, \Omega_n^z$:

$$\Omega_n^x(\mathbf{k}) := \Omega_n^{yz}(\mathbf{k}), \quad \Omega_n^y(\mathbf{k}) := \Omega_n^{zx}(\mathbf{k}), \quad \Omega_n^z(\mathbf{k}) := \Omega_n^{xy}(\mathbf{k}). \quad (30)$$

Eq. (28) can then be rewritten using the definition (30) as

$$\boldsymbol{\Omega}_n(\mathbf{k}) = \begin{pmatrix} \Omega_n^x(\mathbf{k}) \\ \Omega_n^y(\mathbf{k}) \\ \Omega_n^z(\mathbf{k}) \end{pmatrix} = \nabla_{\mathbf{k}} \times \mathbf{d}_{nn}(\mathbf{k}). \quad (31)$$

Properties of the Berry curvature. The Berry curvature can be also written as a summation over eigenstates $n' \neq n$ [3, Eq. (1.13)][43, Eq. (68)]:

$$\Omega_n^{\alpha\beta}(\mathbf{k}) = \sum_{n' \neq n} 2 \operatorname{Im} \left[d_{nn'}^{\alpha}(\mathbf{k}) d_{n'n}^{\beta}(\mathbf{k}) \right]. \quad (32)$$

For a two-band model with valence band v and conduction band c we thus have

$$\Omega_v^{\alpha\beta}(\mathbf{k}) = 2 \operatorname{Im} [d_{vc}^{\alpha}(\mathbf{k}) d_{cv}^{\beta}(\mathbf{k})] = -\Omega_c^{\alpha\beta}(\mathbf{k}). \quad (33)$$

If the system has time-reversal symmetry, we have [3, Eq. (3.8)]

$$\Omega_n^{\alpha\beta}(\mathbf{k}) = -\Omega_n^{\alpha\beta}(-\mathbf{k}). \quad (34)$$

If the system has spatial inversion symmetry, then [3, Eq. (3.9)]

$$\Omega_n^{\alpha\beta}(\mathbf{k}) = \Omega_n^{\alpha\beta}(-\mathbf{k}). \quad (35)$$

Therefore, for crystals with simultaneous time-reversal and spatial inversion symmetry the Berry curvature vanishes identically throughout the Brillouin zone [3],

$$\Omega_n^{\alpha\beta}(\mathbf{k}) = 0. \quad (36)$$

In any case, the sum of the Berry curvature over all bands vanishes,

$$\sum_n \Omega_n^{\alpha\beta}(\mathbf{k}) = 0. \quad (37)$$

Second-order susceptibility. We start by considering a finite system, e.g. a molecule, and its response to a monochromatic electric field $\mathbf{E}(t) = \mathbf{E}(\omega) e^{-i\omega t}$ with frequency ω . The $\chi^{(2)}$ tensor links the electric field with the second-order macroscopic polarization $\mathbf{P}^{(2)}(2\omega)$ at frequency 2ω ,

$$P_\gamma^{(2)}(2\omega) = \sum_{\alpha,\beta} \chi_{\gamma\beta\alpha}^{(2)} E_\beta(\omega) E_\alpha(\omega). \quad (38)$$

We start from Eq. (25) in the SI of Ref. [6],

$$\chi_{\gamma\beta\alpha}^{(2)} = 2C \int_{\text{BZ}} d\mathbf{k} \frac{p_{vc}^\gamma}{\epsilon_{cv} - i/T_2 - 2\omega} \left[\frac{\partial}{\partial k_\beta} \frac{d_{cv}^\alpha}{\epsilon_{cv} - i/T_2 - \omega} + i \frac{d_{cv}^\alpha (d_{cc}^\beta - d_{vv}^\beta)}{\epsilon_{cv} - i/T_2 - \omega} \right], \quad (39)$$

where C is a constant [16], $p_{vc}^\gamma(\mathbf{k}) = -id_{vc}^\gamma(\mathbf{k})\epsilon_{cv}(\mathbf{k})$ [43, Eq. (68)] is the momentum matrix element, $\epsilon_{cv}(\mathbf{k}) = \epsilon_c(\mathbf{k}) - \epsilon_v(\mathbf{k})$ is the energy gap between valence and conduction band at \mathbf{k} and T_2 is the dephasing time. We suppress the k -dependencies of all quantities in Eq. (39). Note that Eq. (39) is not symmetrized for intrinsic permutation symmetry [16] which is of minor importance in our work because the final expressions are symmetric w.r.t. intrinsic permutation symmetry.

Following Ref. [17], we assume both $|\epsilon_{cv} - 2\omega|$ and $1/T_2$ small and $|\epsilon_{cv} - 2\omega| \ll 1/T_2$, such that

$$\begin{aligned} \frac{1}{\epsilon_{cv} - i/T_2 - 2\omega} &= \frac{\epsilon_{cv} - 2\omega}{(\epsilon_{cv} - 2\omega)^2 + 1/T_2^2} + \frac{i/T_2}{(\epsilon_{cv} - 2\omega)^2 + 1/T_2^2} \\ &\stackrel{\epsilon_{cv}-2\omega \rightarrow 0}{=} \frac{i/T_2}{(\epsilon_{cv} - 2\omega)^2 + 1/T_2^2} \stackrel{1/T_2 \rightarrow 0}{=} i \delta(\epsilon_{cv} - 2\omega). \end{aligned} \quad (40)$$

Then, Eq. (39) simplifies for resonant second-harmonic generation $\omega \approx \epsilon_{cv}/2$ and in case of probing a band extremum ($\partial\epsilon_{cv}/\partial k_\beta = 0$) to

$$\chi_{\gamma\beta\alpha}^{(2)} = 2C \int_{\text{BZ}} d\mathbf{k} i \delta(\epsilon_{cv} - 2\omega) \frac{p_{vc}^\gamma}{\epsilon_{cv}/2} \left[\frac{\partial d_{cv}^\alpha}{\partial k_\beta} + i d_{cv}^\alpha (d_{cc}^\beta - d_{vv}^\beta) \right] \quad (41)$$

$$= C \int_{\text{BZ}} d\mathbf{k} \delta(\epsilon_{cv} - 2\omega) \left[d_{vc}^\gamma \frac{\partial d_{cv}^\alpha}{\partial k_\beta} + i d_{vc}^\gamma d_{cv}^\alpha (d_{cc}^\beta - d_{vv}^\beta) \right]. \quad (42)$$

Berry Curvature from differences of the second-order susceptibility. For detecting the k -derivative of the Berry curvature along β direction, we consider

$$\begin{aligned} \text{Im} \left[\chi_{\alpha\beta\gamma}^{(2)} - \chi_{\gamma\beta\alpha}^{(2)} \right] &\stackrel{(42)}{=} C \int_{\text{BZ}} d\mathbf{k} \delta(\epsilon_{cv} - 2\omega) \left(\text{Im} \left[d_{vc}^\alpha \frac{\partial d_{cv}^\gamma}{\partial k_\beta} \right] - \text{Im} \left[d_{vc}^\gamma \frac{\partial d_{cv}^\alpha}{\partial k_\beta} \right] \right. \\ &\quad \left. + \text{Im} [i d_{vc}^\alpha d_{cv}^\gamma - i d_{vc}^\gamma d_{cv}^\alpha] (d_{cc}^\beta - d_{vv}^\beta) \right) \\ &= C \int_{\text{BZ}} d\mathbf{k} \delta(\epsilon_{cv} - 2\omega) \left(\text{Im} \left[d_{vc}^\alpha \frac{\partial d_{cv}^\gamma}{\partial k_\beta} \right] + \text{Im} \left[\left(d_{vc}^\gamma \frac{\partial d_{cv}^\alpha}{\partial k_\beta} \right)^* \right] \right. \\ &\quad \left. + \text{Re} [d_{vc}^\alpha d_{cv}^\gamma - d_{vc}^\gamma d_{cv}^\alpha] (d_{cc}^\beta - d_{vv}^\beta) \right) \\ &= C \int_{\text{BZ}} d\mathbf{k} \delta(\epsilon_{cv} - 2\omega) \left(\text{Im} \left[d_{vc}^\alpha \frac{\partial d_{cv}^\gamma}{\partial k_\beta} \right] + \text{Im} \left[\frac{\partial d_{vc}^\alpha}{\partial k_\beta} d_{cv}^\gamma \right] \right. \\ &\quad \left. + \text{Re} \underbrace{[d_{vc}^\alpha d_{cv}^\gamma - \text{c.c.}]}_{\text{purely imaginary}} \underbrace{(d_{cc}^\beta - d_{vv}^\beta)}_{\text{purely real}} \right) \\ &= C \int_{\text{BZ}} d\mathbf{k} \delta(\epsilon_{cv} - 2\omega) \frac{\partial}{\partial k_\beta} \text{Im} \left[d_{vc}^\alpha d_{cv}^\gamma \right] \stackrel{(33)}{=} \frac{C}{2} \int_{\text{BZ}} d\mathbf{k} \delta(\epsilon_{cv} - 2\omega) \frac{\partial}{\partial k_\beta} \Omega_v^{\alpha\gamma}(\mathbf{k}). \end{aligned}$$

VII. AUTHOR CONTRIBUTIONS STATEMENT

G.S. and J.W. conceived the study, carried out analytical calculations, interpreted the results and wrote the manuscript.

VIII. ACKNOWLEDGMENTS

The authors thank Dr. Kazuki Nakazawa for kindly sharing the raw data of the Berry curvature of t-Te from Ref. [9]. G.S. is deeply grateful to Dr. Manuel Decker for inspiring "Sunday morning" discussions on the concept of chirality, while tirelessly making sandcastles with our kids. J.W. gratefully acknowledges discussions with Ferdinand Evers, Jelena Schmitz, Adrian Seith and Nithin Thomas on topology in ultrafast electron dynamics. G.S. also acknowledges funding by the German Research Foundation DFG (CRC 1375 NOA), project number 398816777 (subproject C4); the International Research Training Group (IRTG) 2675 "Meta-Active", project number 437527638 (subproject A4); and by the Federal Ministry for Education and Research (BMBF) project number 16KIS1792 SiNNER. J.W. acknowledges funding by the DFG via the Emmy Noether Programme (Project No. 503985532), CRC 1277 (project number 314695032, subproject A03) and RTG 2905 (project number 502572516).

IX. DATA AND CODE AVAILABILITY

The data and code that support the plots within this paper and other findings of this study are available from the corresponding author on reasonable request. The code to obtain the Berry curvature derivative from Fig. 2 (c) was executed via Excel.

-
- [1] von Klitzing, K. *et al.* 40 years of the quantum Hall effect. *Nat. Rev. Phys.* **2**, 397–401 (2020).
 - [2] Cai, J. *et al.* Signatures of fractional quantum anomalous Hall states in twisted MoTe₂. *Nature* **622**, 63–68 (2023).
 - [3] Xiao, D., Chang, M.-C. & Niu, Q. Berry phase effects on electronic properties. *Rev. Mod. Phys.* **82**, 1959–2007 (2010).

- [4] Riley, J. M. *et al.* Direct observation of spin-polarized bulk bands in an inversion-symmetric semiconductor. *Nat. Phys.* **10**, 835–839 (2014).
- [5] Mak, K. F., McGill, K. L., Park, J. & McEuen, P. L. The valley Hall effect in MoS₂ transistors. *Science* **344**, 1489–1492 (2014).
- [6] Herrmann, P. *et al.* Nonlinear valley selection rules and all-optical probe of broken time-reversal symmetry in monolayer WSe₂. *Nat. Photonics* (2025). URL <https://doi.org/10.1038/s41566-024-01591-z>.
- [7] Xu, S.-Y. *et al.* Hedgehog spin texture and Berry’s phase tuning in a magnetic topological insulator. *Nat. Phys.* **8**, 616–622 (2012).
- [8] Tsirkin, S. S., Puente, P. A. & Souza, I. Gyrotropic effects in trigonal tellurium studied from first principles. *Phys. Rev. B* **97**, 035158 (2018).
- [9] Nakazawa, K., Yamaguchi, T. & Yamakage, A. Nonlinear charge transport properties in chiral tellurium. *Phys. Rev. Mater.* **8**, L091601 (2024).
- [10] Pan, Y. & Yin, R. Constructing Berry-Maxwell equations with Lorentz invariance and Gauss’s law of Weyl monopoles in four-dimensional energy-momentum space. *Phys. Rev. B* **110**, 075139 (2024).
- [11] Shindou, R. & Balents, L. Artificial electric field in fermi liquids. *Phys. Rev. Lett.* **97**, 216601 (2006).
- [12] Boyd, R. W. *Nonlinear Optics* (Academic Press, 2008), 3rd edn.
- [13] Fiebig, M. *Nonlinear Optics on Ferroic Materials* (Wiley-VCH, 2023), 1st edn.
- [14] See Refs. [3, 15] and online methods for details.
- [15] Yue, L. & Gaarde, M. B. Introduction to theory of high-harmonic generation in solids: tutorial. *J. Opt. Soc. Am. B* **39**, 535–555 (2022).
- [16] Aversa, C. & Sipe, J. E. Nonlinear optical susceptibilities of semiconductors: Results with a length-gauge analysis. *Phys. Rev. B* **52**, 14636–14645 (1995).
- [17] Morimoto, T. & Nagaosa, N. Topological nature of nonlinear optical effects in solids. *Sci. Adv.* **2**, e1501524 (2016).
- [18] A similar result as Eq. (3) was derived from Keldysh Green’s functions combined with the Floquet formalism [17, Eq. (20)]; we present our derivation based on perturbative solutions of Semiconductor Bloch Equations (SBE) [6, 16] in the online methods.
- [19] See Ref. [3] and online methods.

- [20] Sodemann, I. & Fu, L. Quantum Nonlinear Hall Effect Induced by Berry Curvature Dipole in Time-Reversal Invariant Materials. *Phys. Rev. Lett.* **115**, 216806 (2015).
- [21] Mak, K. F., Xiao, D. & Shan, J. Light–valley interactions in 2d semiconductors. *Nat. Photonics* **12**, 451–460 (2018).
- [22] Fecher, G. H., Kübler, J. & Felser, C. Chirality in the solid state: Chiral crystal structures in chiral and achiral space groups. *Materials* **15**, 5812 (2022).
- [23] Hahn, T., Klapper, H., Müller, U. & Aroyo, M. I. *Point groups and crystal classes*, chap. 3.2, 720–776 (John Wiley & Sons, Ltd, 2016).
- [24] Baumgartner, C. *et al.* Supercurrent rectification and magnetochiral effects in symmetric Josephson junctions. *Nat. Nanotechnol.* **17**, 39–44 (2022).
- [25] Evers, F. *et al.* Theory of chirality induced spin selectivity: Progress and challenges. *Adv. Mater.* **34**, 2106629 (2022).
- [26] Chen, Y. *et al.* Multidimensional nanoscopic chiroptics. *Nat. Rev. Phys.* **4**, 113–124 (2022).
- [27] Chen, Y. *et al.* Observation of intrinsic chiral bound states in the continuum. *Nature* **613**, 474–478 (2023).
- [28] Chang, G. *et al.* Topological quantum properties of chiral crystals. *Nat. Mater.* **17**, 978–985 (2018).
- [29] Gatti, G. *et al.* Radial Spin Texture of the Weyl Fermions in Chiral Tellurium. *Phys. Rev. Lett.* **125**, 216402 (2020).
- [30] Gosálbez-Martínez, D., Crepaldi, A. & Yazyev, O. V. Diversity of radial spin textures in chiral materials. *Phys. Rev. B* **108**, L201114 (2023).
- [31] Hirayama, M., Okugawa, R., Ishibashi, S., Murakami, S. & Miyake, T. Weyl Node and Spin Texture in Trigonal Tellurium and Selenium. *Phys. Rev. Lett.* **114**, 206401 (2015).
- [32] Cheng, M., Wu, S., Zhu, Z.-Z. & Guo, G.-Y. Large second-harmonic generation and linear electro-optic effect in trigonal selenium and tellurium. *Phys. Rev. B* **100**, 035202 (2019).
- [33] Note that for point groups $C_n, D_n, n \geq 3$, we have $\chi_{xzy}^{(2)} = -\chi_{yzx}^{(2)}$ which is needed for evaluating Eq. (20).
- [34] Schröter, N. B. M. *et al.* Observation and control of maximal chern numbers in a chiral topological semimetal. *Science* **369**, 179–183 (2020).
- [35] Yen, Y. *et al.* Controllable orbital angular momentum monopoles in chiral topological semimetals. *Nat. Phys.* **20**, 1912–1918 (2024).

- [36] Bloembergen, N. Conservation laws in nonlinear optics. *J. Opt. Soc. Am.* **70**, 1429–1436 (1980).
- [37] Schüler, M. *et al.* Local Berry curvature signatures in dichroic angle-resolved photoelectron spectroscopy from two-dimensional materials. *Sci. Adv.* **6**, eaay2730 (2020).
- [38] Ma, J. & Pesin, D. A. Chiral magnetic effect and natural optical activity in metals with or without Weyl points. *Phys. Rev. B* **92**, 235205 (2015).
- [39] Resta, R. & Vanderbilt, D. *Theory of Polarization: A Modern Approach*, 31–68 (Springer Berlin Heidelberg, Berlin, Heidelberg, 2007).
- [40] Felser, C. & Gooth, J. *Topology and Chirality*, 115–141 (2023).
- [41] Bhalla, P., Das, K., Culcer, D. & Agarwal, A. Resonant Second-Harmonic Generation as a Probe of Quantum Geometry. *Phys. Rev. Lett.* **129**, 227401 (2022).
- [42] Orenstein, J. *et al.* Topology and symmetry of quantum materials via nonlinear optical responses. *Ann. Rev. Condens. Matter Phys.* **12**, 247–272 (2021).
- [43] Wilhelm, J. *et al.* Semiconductor Bloch-equations formalism: Derivation and application to high-harmonic generation from Dirac fermions. *Phys. Rev. B* **103**, 125419 (2021).